# 1 Supplementary material for LHCb-PAPER-2014-006

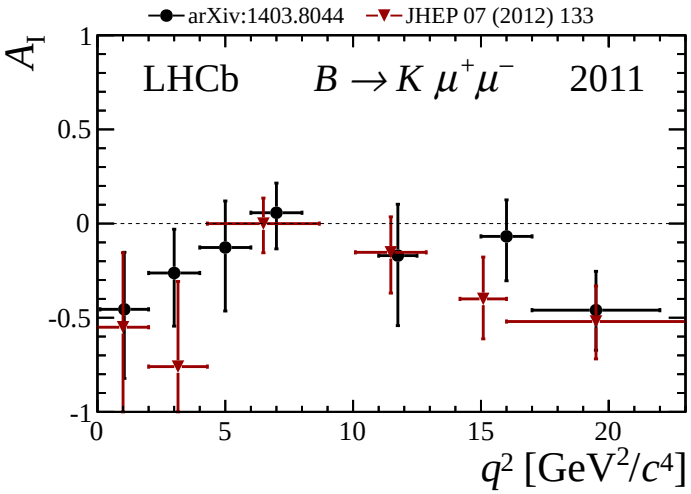


Figure 1: Isospin asymmetry results for $B \to K\mu^+\mu^-$ obtained in this analysis (LHCb-PAPER-2014-006) and an earlier analysis (JHEP 07 (2012) 133) [1]. Both measurements only use the 2011 dataset. These two measurements use data samples that have different reconstruction algorithms and event selection. A $\chi^2$ test on the compatibility of the two results, taking the overlap of events into account, has a $p$-value of 93%.

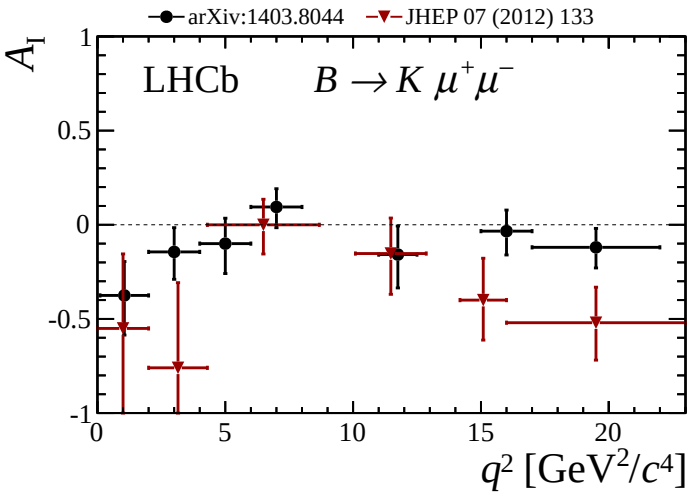


Figure 2: Isospin asymmetry results for $B \to K\mu^+\mu^-$ obtained in this analysis (LHCb-PAPER-2014-006) and an earlier analysis (JHEP 07 (2012) 133) [1]. These two analyses use data samples that have different reconstruction algorithms and event selection.

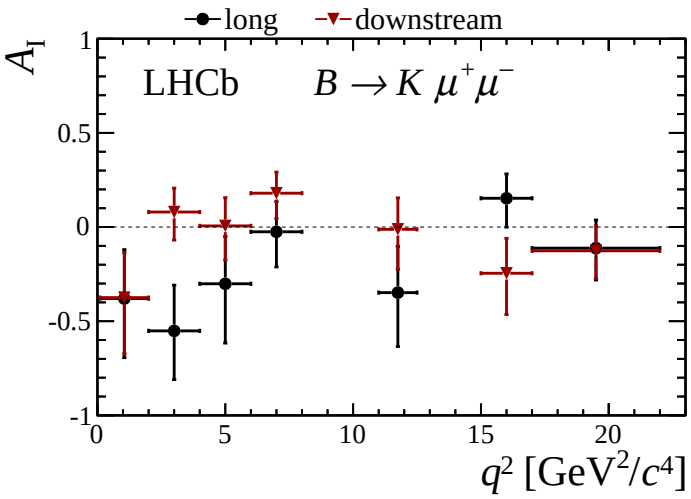


Figure 3: Isospin asymmetry results for $B \to K\mu^+\mu^-$ split between the long and downstream $K^0_S$ reconstruction categories. A $\chi^2$ compatibility test between the long and downstream categories gives a $p$-value of 15%.

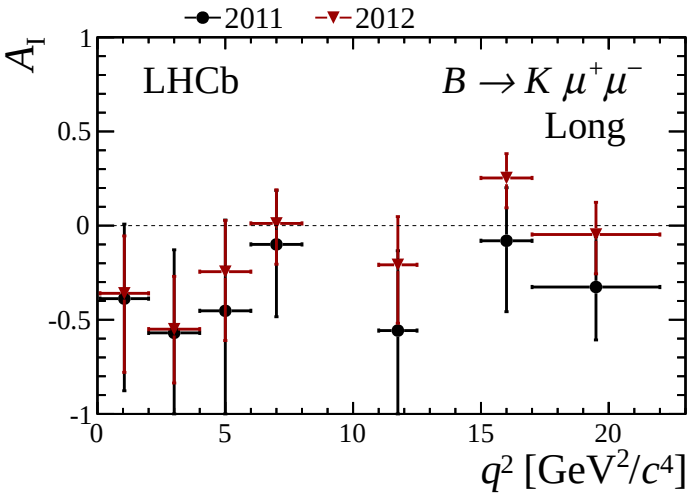


Figure 4: Isospin asymmetry of $B \to K\mu^+\mu^-$ obtained separately from the 2011 and 2012 data sets for the long $K^0_S$ reconstruction category.

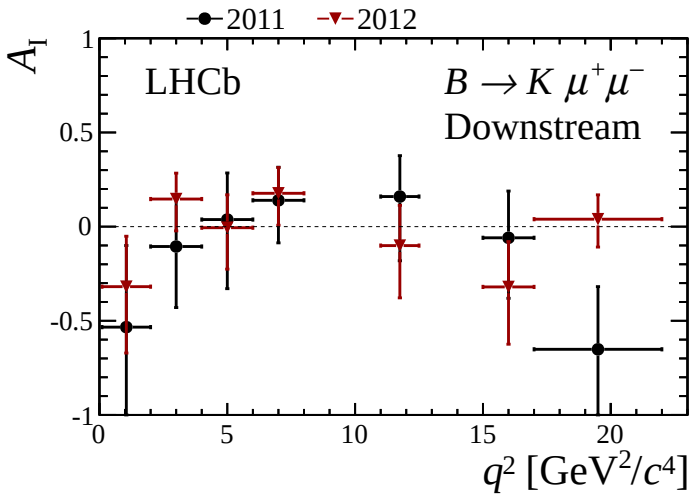


Figure 5: Isospin asymmetry of $B \to K\mu^+\mu^-$ obtained separately from the 2011 and 2012 data sets for the downstream $K^0_S$ reconstruction category.

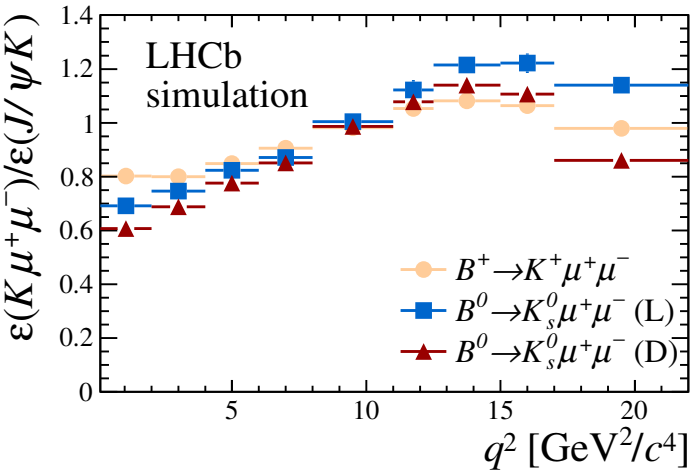


Figure 6: Relative efficiency as a function of $q^2$ for for $B \to K\mu^+\mu^-$ decays. For the $B^0 \to K^0\mu^+\mu^-$ mode, it is broken up into the long (L) and downstream (D) categories of the reconstructed $K^0_S$, respectively.

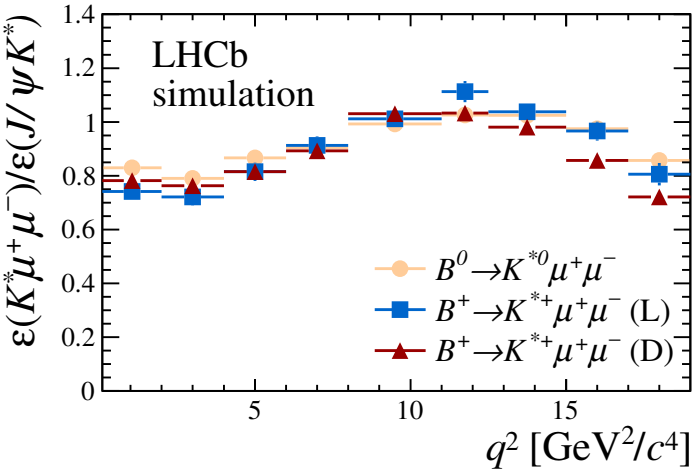


Figure 7: Relative efficiency as a function of $q^2$ for $B \to K^*\mu^+\mu^-$ decays. For the $B^+ \to K^{*+}\mu^+\mu^-$ mode, it is broken up into the long (L) and downstream (D) categories of the reconstructed $K^0_S$, respectively

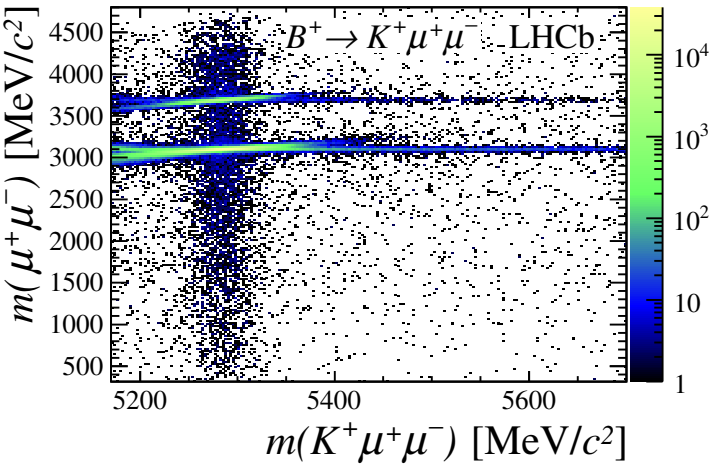


Figure 8: Selected $B^+ \to K^+\mu^+\mu^-$ candidates versus $K^+\mu^+\mu^-$ and $\mu^+\mu^-$ mass of selected in bins of 5.3 MeV/$c^2$ by 45 MeV/$c^2$.

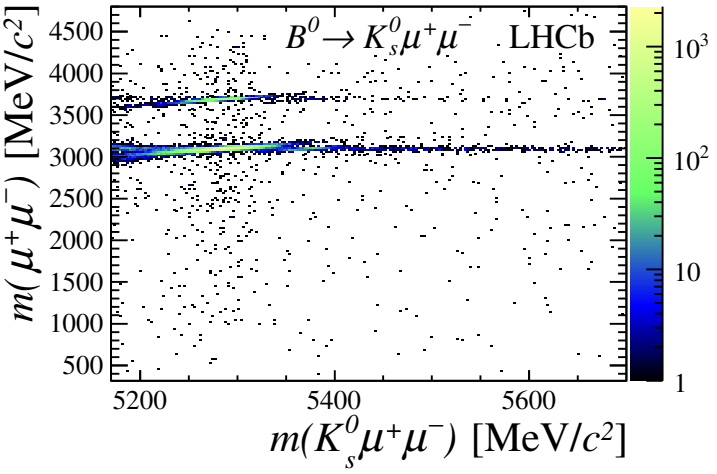


Figure 9: Selected $B^0 \to K^0_S \mu^+\mu^-$ candidates versus $K^0_S \mu^+\mu^-$and $\mu^+\mu^-$ mass of selected in bins of 5.3 MeV/$c^2$ by 45 MeV/$c^2$.

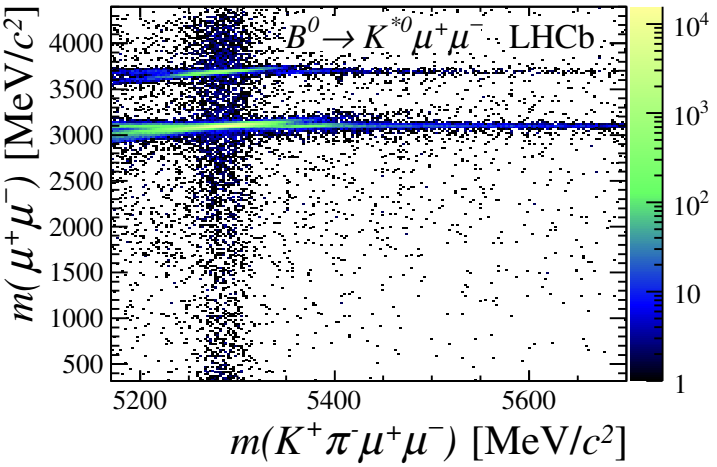


Figure 10: Selected $B^0 \to K^{*0}\mu^+\mu^-$ candidates versus $K^+\pi^-\mu^+\mu^-$ and $\mu^+\mu^-$ mass of selected in bins of 5.3 MeV/$c^2$ by 45 MeV/$c^2$.

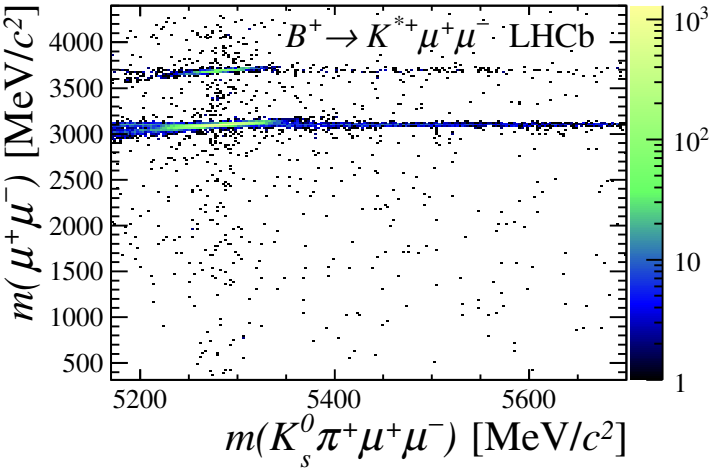


Figure 11: Selected $B^+ \to K^{*+}\mu^+\mu^-$ candidates versus $K^0_S\pi^+\mu^+\mu^-$ and $\mu^+\mu^-$ mass of selected in bins of 5.3 MeV/$c^2$ by 45 MeV/$c^2$.

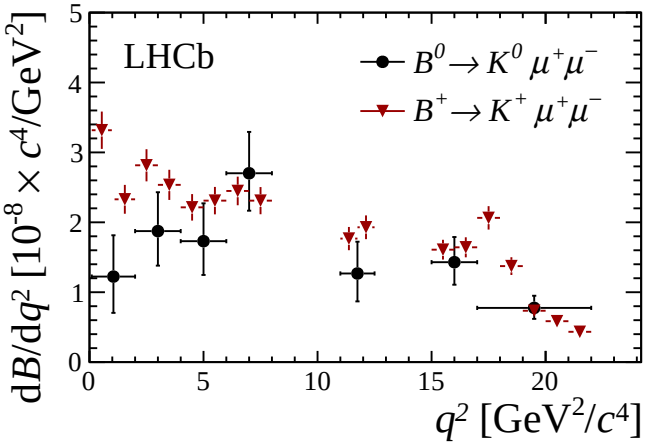


Figure 12: $B^+ \to K^+\mu^+\mu^-$ and $B^0 \to K^0\mu^+\mu^-$ branching fractions overlaid.

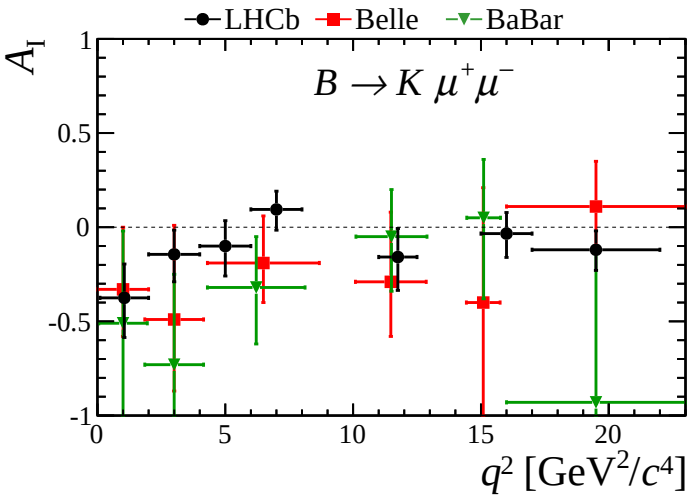


Figure 13: Isospin asymmetry for $B \to K\mu^+\mu^-$ as measured by LHCb, BaBar [2] and Belle [3].

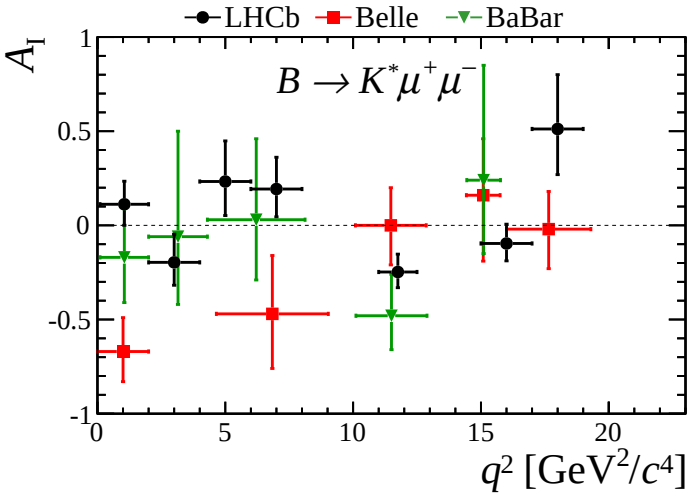


Figure 14: Isospin asymmetry for $B \to K^*\mu^+\mu^-$ as measured by LHCb, BaBar [2] and Belle [3].

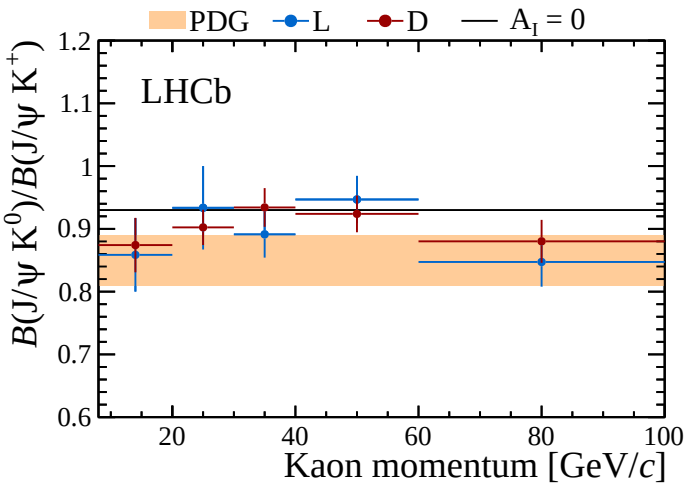


Figure 15: Ratio of $B^0 \to J/\psi K^0$ to $B^+ \to J/\psi K^+$ branching fractions after the $K^0_S$ efficiency corrections described in the paper are applied. Uncertainties are statistical only. The band shows the PDG value and its uncertainty. The data points are for long (L) and downstream (D) categories of the reconstructed $K^0_S$, respectively. The $A_I = 0$ line corresponds to the expectation if there is no isospin asymmetry between the decays.

# References


[1] LHCb collaboration, R. Aaij *et al.*, *Measurement of the isospin asymmetry in $B \to K^{(*)}\mu^+\mu^-$ decays*, JHEP **07** (2012) 133, arXiv:1205.3422.

[2] BaBar collaboration, B. Aubert *et al.*, *Measurement of branching fractions and rate asymmetries in the rare decays $B \to K^{(*)}\ell^+\ell^-$*, Phys. Rev. **D86** (2012) 032012, arXiv:hep-ex/1204.3933.

[3] Belle collaboration, J.-T. Wei *et al.*, *Measurement of the differential branching fraction and forward-backward asymmetry for $B \to K^{(*)}l^+l^-$*, Phys. Rev. Lett. **103** (2009) 171801, arXiv:0904.0770.